21 Modulation

David M. Beams
University of Texas at Tyler

21.1 Introduction

It is often the case in instrumentation and communication systems that an information-bearing signal may not be in an optimal form for direct use. In such cases, the information-bearing signal may be used to alter some characteristic of a second signal more suited to the application. This process of altering one signal by means of another is known as **modulation**; the original information is called the *baseband signal*, and the signal modulated by the baseband signal is termed the *carrier* (because it "carries" the information). Recovery of the original information requires a suitable demodulation process to reverse the modulation process.

A prominent use of modulation techniques is found in radio communication. The extremely long wavelengths of electromagnetic waves at frequencies found in a typical audio signal make direct transmission impractical, because of constraints on realistic antenna size and bandwidth. Successful radio communication is made possible by using the original audio (baseband) signal to modulate a carrier signal of a much higher frequency and transmitting the modulated carrier by means of antennas of feasible size. Another example is found in the use of modems to transmit digital data by the telephone network. Digital data are not directly compatible with analog local subscriber connections, but these data may be used to modulate audible signals which may be carried over local telephone lines. Instrumentation systems use modulation techniques for telemetry (where the distances may be on the order of centimeters for implanted medical devices to hundreds of millions of kilometers for deep-space probes), for processing signals in ways for which the original signals are unsuited (such as magnetic recording of low-frequency and dc signals), and for specialized amplification purposes (carrier and lock-in amplifiers).

Techniques that modulate the amplitude of the carrier are full-carrier **amplitude modulation** (AM), reduced- or suppressed-carrier double-sideband amplitude modulation (DSB), single-sideband suppressed-carrier modulation (SSB), vestigial-sideband modulation (VSB), and on–off keying (OOK). Techniques that modulate the frequency or phase angle of the carrier include **frequency modulation** (FM), phase modulation (PM), frequency-shift keying (FSK), and phase-shift keying (PSK). Simultaneous variation

of amplitude and phase are applied in quadrature amplitude modulation (QAM). Each technique has its own particular uses. Full-carrier AM is used in radio broadcasting; VSB is used in television broadcasting. DSB appears in instrumentation systems utilizing carrier amplifiers and modulating sensors, while SSB finds use in certain high-frequency radio communications. FM is used in broadcasting (radio and television audio) and point-to-point mobile communications. OOK is commonly used to transmit digital data in optical fiber links. FSK, PSK, and QAM are found in digital communications; analog QAM carries the chrominance (color) information in color television broadcasting. The emphasis of this particular chapter will be instrumentation systems; those interested principally in communications applications could begin by consulting References 1 through 4.

21.2 Generalized Modulation

We begin by making two assumptions: (1) the highest frequency present in the baseband signal is considerably less than the carrier frequency and (2) the results derived in the following chapter pertain to sinusoidal carriers but may be extended to other periodic carrier signals (such as square waves and triangle waves). Equation 21.1 gives a general expression for a modulated sinusoidal carrier signal of radian frequency ω_c:

$$f_s(t) = A_c(t)\cos\left[\omega_c t + \phi(t)\right] \tag{21.1}$$

Information may be carried by $f_s(t)$ by modulation of its amplitude $A_c(t)$, its phase angle $\phi(t)$, or, in some cases, both (note that frequency modulation is a form of phase **angle modulation**). Equation 21.1 may be recast in an equivalent form:

$$f_s(t) = f_i(t)\cos(\omega_c t) - f_q(t)\sin(\omega_c t) \tag{21.2}$$

where:

$$f_i(t) = A_c(t)\cos\left[\phi(t)\right]$$

$$f_q(t) = A_c(t)\sin\left[\phi(t)\right]$$

Equation 21.2 gives $f_s(t)$ as the sum of a cosinusoidal carrier term with time-varying amplitude $f_i(t)$ and a sinusoidal (quadrature) carrier term with time-varying amplitude $f_q(t)$ and is thus known as the carrier-quadrature description of $f_s(t)$. The terms $f_i(t)$ and $f_q(t)$ are known, respectively, as the in-phase and quadrature components of $f_s(t)$. Carlson [1] gives the Fourier transform of a signal in carrier-quadrature form:

$$F_s(\omega) = \frac{1}{2}\left[F_i(\omega - \omega_c) + F_i(\omega + \omega_c)\right] + \frac{j}{2}\left[F_q(\omega - \omega_c) + F_q(\omega + \omega_c)\right] \tag{21.3}$$

where $F_i(\omega)$: $f_i(t)$ and $F_q(\omega)$: $f_q(t)$ are Fourier transform pairs. Notice that the spectra of both $F_i(\omega)$ and $F_q(\omega)$ are both translated by $\pm\omega_c$. Modulation of the carrier in any sense causes energy to appear at frequencies (known as *sidebands*) other than the carrier frequency. Sidebands will be symmetrically distributed relative to the carrier in all but the specialized cases of VSB and SSB.

21.3 Amplitude Modulation

AM that appears in instrumentation systems takes the form of double-sideband AM on which we will focus some degree of attention. VSB and SSB are encountered in communications systems but not in instrumentation systems; interested readers may refer to References 1 through 3.

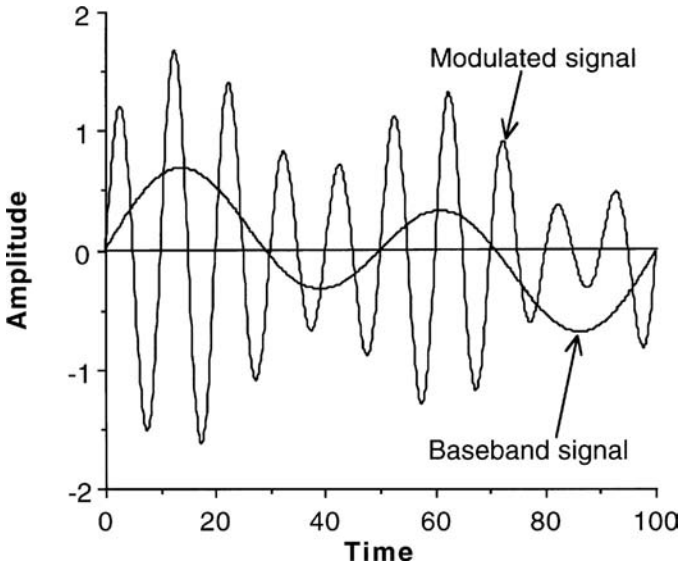

FIGURE 21.1 Time-domain representation of a baseband and the resulting full-carrier AM signal. The time scale is arbitrary.

Double-Sideband Amplitude Modulation

AM applied to a sinusoidal carrier is described by

$$f_s(t) = A_c\left[k + \mu f_m(t)\right]\cos\left(\omega_c t\right) \tag{21.4}$$

where A_c is the amplitude of the unmodulated carrier, k is the proportion of carrier present in the modulated signal, μ is the modulation index, $f_m(t)$ is the modulating baseband signal (presumed to be a real bandpass signal), and ω_c is the carrier radian frequency. The modulation index relates the change in amplitude of the modulated signal to the amplitude of the baseband signal. The value of k ranges from 1 in full-carrier AM to 0 in suppressed-carrier double-sideband modulation. The peak value of the modulated signal is $k + \mu f_m(t)$ which may take on any positive value consistent with the dynamic range of the modulator and demodulating system; note that phase reversal of the carrier occurs if $k + \mu f_m(t)$ becomes negative. Figure 21.1 represents a full-carrier AM signal and its baseband signal. Recasting Equation 21.4 in carrier-quadrature form gives $f_i = A_c[k + \mu f_m(t)]$ and $f_q = 0$. The Fourier transform of this signal is

$$F_s(\omega) = \frac{A_c}{2}\left\{k\delta\left(\omega - \omega_c\right) + k\delta\left(\omega + \omega_c\right) + \mu\left[F_m\left(\omega - \omega_c\right) + F_m\left(\omega + \omega_c\right)\right]\right\} \tag{21.5}$$

where $\delta(\omega - \omega_c)$ and $\delta(\omega + \omega_c)$ are unit impulses at $+\omega_c$ and $-\omega_c$, respectively, and represent the carrier component of $F_S(\omega)$. The frequency domain representation of $F_S(\omega)$ also contains symmetric sidebands about the carrier with the upper sideband arising from the positive-frequency component of $F_m(\omega)$ and the lower sideband from the negative-frequency component. A double-sideband AM signal thus has a bandwidth twice as large as that of the baseband signal.

Figure 21.2 shows a time-domain representation of a suppressed-carried DSB signal with the same baseband modulation as in Figure 21.1. The information in a full-carrier AM signal is found in the

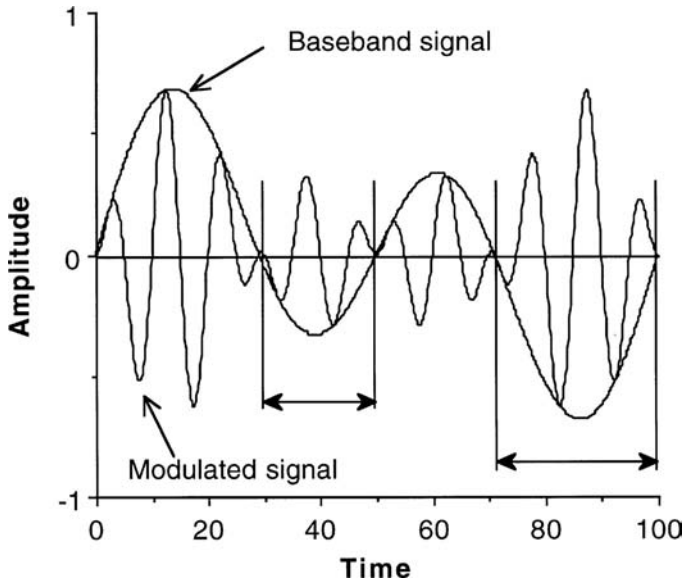

FIGURE 21.2 Time-domain representation of a DSB suppressed-carrier signal. Regions demarcated by double arrows indicate phase inversion of the modulated signal relative to the unmodulated carrier. This is in contrast to full-carrier AM in which the modulated signal is always in phase with the carrier.

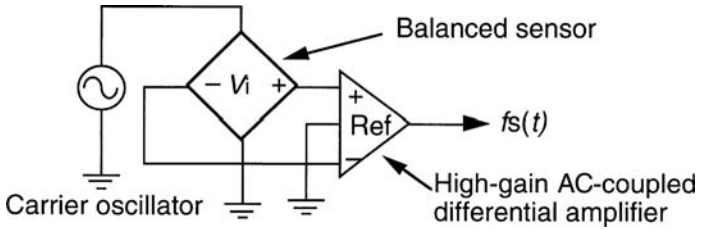

FIGURE 21.3 A balanced sensor with ac excitation and a differential-amplifier output stage. Typical sensors which might be found in this role are resistive Wheatstone bridges, differential-capacitance pressure sensors or accelerometers, or linear-variable differential transformers (LVDTs). Variation in the sensor measurand produces a DSB suppressed-carrier signal at the amplifier output.

time-varying amplitude of the modulated signal, but the information carried by the suppressed-carrier DSB signal is found both in the amplitude and instantaneous phase of the modulated signal (note that the phase of the DSB signal is inverted relative to the carrier when the baseband signal is negative and in phase when the baseband signal is positive). AM is a linear modulation technique; the sum of multiple AM signals produced from a common carrier by different baseband signals is the same as one AM signal produced by the sum of the baseband signals.

Generation of Double-Sideband AM Signals

AM in radio transmitters is frequently performed by applying the modulating waveform to the supply voltage to a nonlinear radiofrequency power amplifier with a resonant-circuit load as described by Carlson [1]. Low-level AM may be achieved by direct multiplication of the carrier signal by $[k + \mu f_m(t)]$.

AM signals often arise in instrumentation systems as the result of the use of an ac drive signal to a modulating sensor. Figure 21.3 shows an example in which a balanced sensor is excited by a sinusoidal carrier. The output voltage of the differential amplifier will be zero when the sensor is balanced; a nonzero

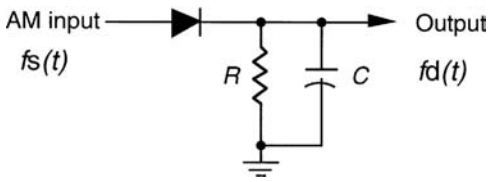

FIGURE 21.4 Envelope detector for full-carrier AM signals.

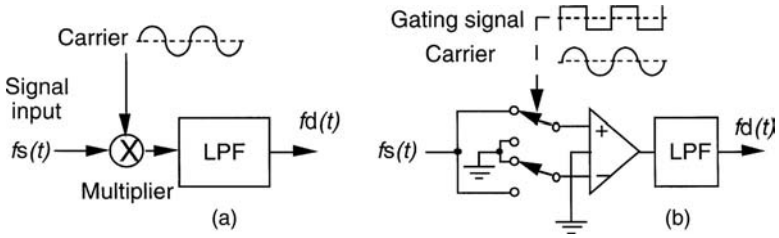

FIGURE 21.5 Multiplying (a) and switching (b) synchronous demodulators. The blocks marked **LPF** represent low-pass filters.

output voltage appears when the sensor is unbalanced. The magnitude of the voltage indicates the degree of imbalance in the sensor, and the phase of the output voltage relative to the carrier determines the direction of imbalance. The suppressed-carrier DSB signal of Figure 21.2 would be seen at the amplifier output if we substitute the sensor measurand for the baseband signal of Figure 21.2. The technique of applying ac excitation to a balanced sensor may be required for inductive or capacitive sensors; it may also be desirable in the case of resistive sensors (such as strain-gage bridges) requiring high-gain amplifiers. In these circumstances, amplification of an ac signal minimizes both $1/f$ noise and dc offset problems associated with high-gain dc-coupled amplifiers.

Envelope Demodulation of Double-Sideband AM Signals

Full-carrier AM signals are readily demodulated by the simple envelope detector shown in Figure 21.4. The components of the *RC* low-pass filter are chosen such that $\omega_m \ll (1/RC) \ll \omega_c$. Envelope detection, however, cannot discriminate phase and is thus unsuitable for demodulation of signals in which phase reversal of the carrier occurs (such as reduced-carrier or suppressed-carrier signals). Synchronous demodulation is required for such signals.

Synchronous Demodulation of Double-Sideband AM Signals

Figure 21.5 shows two methods of synchronous demodulation. In Figure 21.5(a), the modulated signal is multiplied by $\cos(\omega_c t)$; in Figure 21.5(b), the modulated signal is gated by a square wave synchronous with $\cos(\omega_c t)$. Consider the multiplying circuit of Figure 21.5(a); the Fourier transform $F_d(\omega)$ of $f_d(t) = f_s(t)\cos(\omega_c t)$ is given by

$$F_d(\omega) = \frac{(A_c k)}{4}\left[\delta(\omega - 2\omega_c) + \delta(\omega + 2\omega_c) + 2\delta(\omega)\right] + \frac{(\mu A_c)}{4}\left[F_m(\omega - 2\omega_c) + F_m(\omega - 2\omega_c) + 2F_m(\omega)\right] \quad (21.6)$$

The spectral components translated by $\pm 2\omega_c$ may be removed by low-pass filtering; the result, translated into the time domain, is

$$f_d(t) = \frac{A_c k}{2} + \frac{\mu A_c}{2} f_m(t) \quad (21.7)$$

We thus have a dc component of $A_c k/2$ and the original baseband signal $f_m(t)$ multiplied by a scale factor of $\mu A_c/2$. The gating circuit of Figure 21.5(b) may be analyzed in a similar manner; the action of gating is equivalent to multiplying $f_s(t)$ by a square wave with levels of ±1. The Fourier series representation of such a square wave is given by

$$f_g(t) = \frac{4}{\pi}\sum_{n=0}^{\infty}\frac{(-1)^n}{(2n+1)}\cos\left[(2n+1)\omega_c t\right] \tag{21.8}$$

Low-pass filtering of the product of Equations 21.4 and 21.8 gives

$$f_d(t) = \frac{2A_c k}{\pi} + \frac{2\mu A_c}{\pi} f_m(t) \tag{21.9}$$

The baseband signal is again recovered, although the scale factor is somewhat larger than that of the multiplying case. Demodulators like those of Figure 21.5(a) are called multiplying demodulators; circuits Figure 21.5(b) are known as switching demodulators. Nowicki [5] and Meade [6] discuss and compare both types of synchronous demodulators in greater detail.

We have so far made the implicit assumption that the demodulating signal is perfectly synchronized with the carrier of the modulated signal. Let us now consider the case where there exists a phase shift between these two signals. Assume that a signal expressed in carrier-quadrature form is multiplied by a demodulating signal $\cos(\omega_c t + \theta)$. The result, after suitable low-pass filtering, is

$$f_d(t) = \frac{f_i(t)}{2}\cos(\theta) + \frac{f_q(t)}{2}\sin(\theta) \tag{21.10}$$

Equation 21.10 is an important result; we see that both the level and polarity of the demodulated signal are functions of the synchronization between the demodulating signal and the modulated carrier. Synchronous demodulation is thus often called phase-sensitive demodulation. It was previously mentioned that a DSB AM signal has no quadrature component $f_q(t)$; a phase shift of an odd integral multiple of $\pi/2$ radians between the carrier and the demodulating signal will produce a synchronous demodulator output of zero. Use of a square wave gating signal in place of the sinusoid would produce the same result as Equation 21.10 except that the recovered signals would be multiplied by $2/\pi$ instead of 1/2.

Figure 21.6 shows the effect of phase between the gating signal and the incoming signal in a switching phase-sensitive demodulator. A sinusoid with a constant amplitude of 1 is gated by a square wave which has levels of ±1; the amplifier outputs before low-pass filtering are shown for phase offsets of 0, $\pi/4$, and $\pi/2$ radians. The dc levels which would be recovered by low-pass filtering are also shown. Note that the demodulator output with phase offset of zero takes the form of a full-wave rectified sine which has only positive excursions. As the phase offset between the gating signal and the sinusoid increases, however, the dc component decreases as the gated signal shows increasing negative excursions and decreasing positive excursions. An offset of $\pi/2$ radians produces an output whose positive and negative excursions are symmetric and thus has no dc component. Synchronization of the demodulating signal with the modulated carrier is thus crucial for accurate demodulation. Synchronization of the demodulating signal with the modulated carrier is straightforward in instrumentation applications in which the carrier signal may be provided directly to the demodulator, such as the electrical impedance tomography applications discussed by Webster [7]. This becomes more difficult if the carrier cannot be directly provided but must be inferred or recovered from the incoming signal. Hershberger [8] employs a phase-locked loop to perform the carrier synchronization in a synchronous detector for radio receiver applications. Modulated signals which contain both in-phase and quadrature components may be demodulated by an I–Q demodulator which is comprised of two parallel synchronous demodulators (one driven by $\cos(\omega_c t)$ and the other by $\sin(\omega_c t)$); Breed [9] notes that any form of modulation may in principle be demodulated

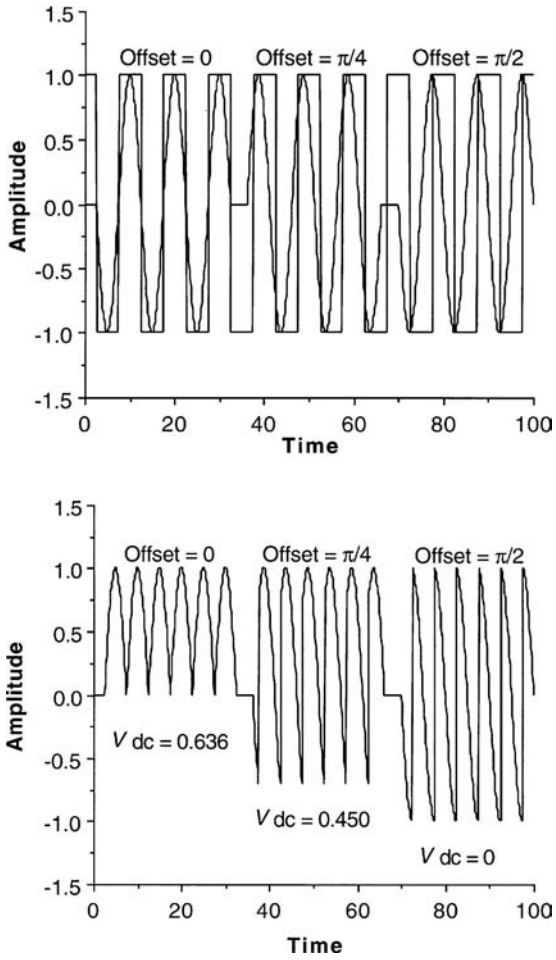

FIGURE 21.6 Gating of a constant-amplitude sinusoidal by a square wave in a switching phase-sensitive demodulator with various phase offsets between the carrier and the square wave. The upper trace shows the carrier and the square wave; the lower trace shows the signals which appear at the output of the differential amplifier in Figure 21.5(b). The dc output voltages of the low-pass filter are indicated for each value of phase offset.

by this method although less expensive techniques are suitable for many applications (such as the envelope detector for full-carrier AM). A common instrumentation application for simultaneous I–Q demodulation is the electrical impedance bridge (often called an *LCR* bridge).

Synchronous demodulators are valuable in lock-in amplifier applications for the recovery of signals otherwise masked by noncoherent noise. Assume that the low-pass filter of a synchronous demodulator has a bandwidth of Ω; only those components of the incoming signal which lie within $\pm\Omega$ of ω_c will appear at the low-pass filter output. A demodulator with extremely high selectivity may be built by use of a narrow low-pass filter, providing remarkable improvement in output signal-to-noise ratio. The use of an AD630 switching demodulator to recover a signal from broadband noise whose rms value is 100 dB greater than that of the modulated signal is shown in Reference 10. Synchronous demodulation may also be of benefit in applications in which the input signal-to-noise ratio is not so extreme; components of noise which are in quadrature with respect to the carrier produce no output from a synchronous demodulator, whereas an envelope detector responds to the instantaneous sum of the signal and all noise components.

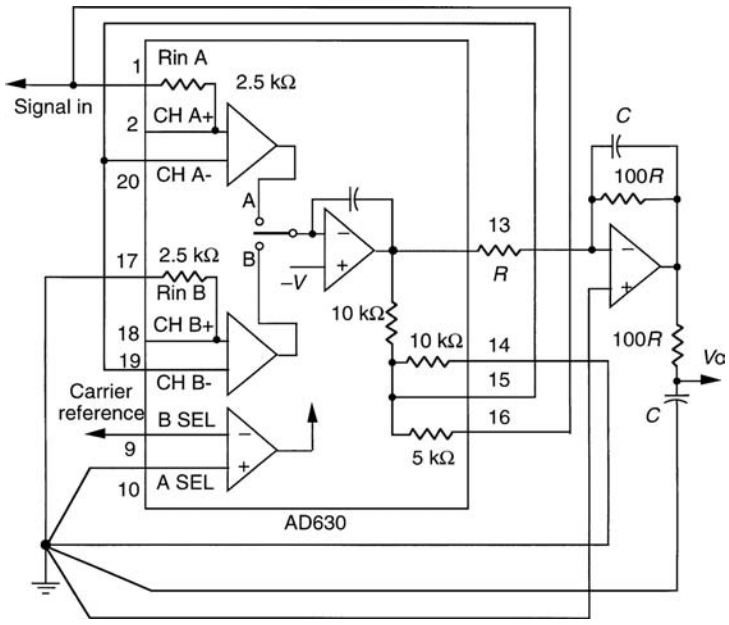

FIGURE 21.7 Lock-in amplifier circuit utilizing the Analog Devices AD630 switching balanced demodulator. This particular device is attractive for the small number of external components required and its high performance. The two-pole low-pass filter shown has a dc gain of 100 and a corner frequency of 0.00644/*RC*. The principal drawback of this filter is its dc output impedance which is 100*R*. This limitation could be avoided by replacing this filter by a pair of single-pole active filters or a single-amplifier two-pole filter (such as the Sallen-Key type of network). Resistances depicted within the outline of the AD630 are internal to the device itself; numbers at the periphery of the device are pin numbers. Pins labeled CH A+, CH A–, CH B+, and CH B– indicate the sense of the A and B channels of the device. Pins Rin A and Rin B are electrically connected to the CH A+ and CH B+ pins, respectively, through internal 2.5 kΩ resistances.

Examples

Figure 21.7 shows a lock-in amplifier application of the AD630; this particular integrated circuit has on-chip precision resistances which allow the device to be used with a minimal number of external components. Webster [11] shows the design of a diode-ring phase-sensitive demodulator. High-speed CMOS switches (such as the 74HC4053 and ADG201HS) may also be used in switching phase-sensitive demodulators. An example of this is shown in Figure 21.8 below in which presents a method for measurement of both amplitude and phase of a sinusoidal ac voltage. This method requires that gating signals synchronous with $\cos(\omega t)$ and $\sin(\omega t)$ be supplied to a pair of independent single-pole, single-throw switches. Assuming that the input signal V_{in} may be represented as $A\cos(\omega t+\varphi)$, the dc output voltages from the two *RC* low-pass filters are given by:

$$V_{OI} = \frac{A}{\pi}\cos(\phi) \tag{21.11a}$$

$$V_{OQ} = \frac{-A}{\pi}\sin(\phi) \tag{21.11b}$$

where the phase angle φ is measured relative to $\cos(\omega t)$. Note that switching the input of the low-pass filter between the signal and ground produces dc output voltages half as large as those produced by the technique of Figure 21.5(b). The amplitude A and phase φ of the signal may be readily computed from V_{OI} and V_{OQ}:

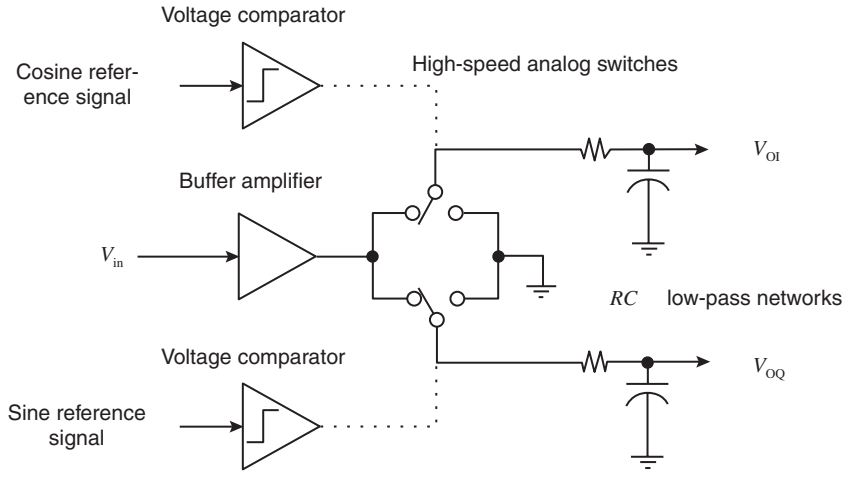

FIGURE 21.8 Use of phase-sensitive detection to measure amplitude and phase of a sinusoidal signal. Phase is measured with respect to $\cos(\omega t)$.

$$A = \pi\sqrt{V_{OI}^2 + V_{OQ}^2} \tag{21.12a}$$

$$\phi = \tan^{-1}\left(\frac{-V_{OQ}}{V_{OI}}\right) \tag{21.12b}$$

Beams [12] applies this technique with a virtual-instrument program to the automated measurement of frequency response of linear networks.

21.4 Angle (Frequency and Phase) Modulation

Recall from Equation 21.1 that we may modulate a carrier by varying its phase angle in accordance with the baseband signal. Consider a signal of the form:

$$f_s(t) = A_c \cos\left[\omega_c t + \Delta\phi x_m(t)\right] \tag{21.13}$$

The instantaneous phase angle is $\omega_c t + \Delta\phi x_m(t)$; the phase relative to the unmodulated carrier is $\Delta\phi x_m(t)$. The carrier is thus phase-modulated by $x_m(t)$. The instantaneous frequency is $\omega_c + \Delta\phi[dx_m(t)/dt]$; if $x_m(t)$ is the integral of baseband signal $f_m(t)$, the instantaneous frequency becomes $\omega_c + \Delta\phi f_m(t)$. The frequency deviation $\Delta\phi f_m(t)$ is proportional to the baseband signal; the carrier is frequency modulated by $f_m(t)$. We may write the general expression for an FM signal as

$$f_s(t) = A_c \cos\left[\omega_c t + \Delta\omega \int_{-\infty}^{t} f_m(\tau)d\tau\right] \tag{21.14}$$

(The change in notation from $\Delta\phi$ to $\Delta\omega$ is intended to emphasize that the signal represented by Equation 21.14 is frequency modulated.) Figure 21.9 shows a time-domain representation of an FM signal. Note the signal has constant amplitude; this is also true of a phase-modulated signal.

Consider frequency modulation with a baseband signal $f_m = A_m \cos(\omega_m t)$; substitution into Equation 21.14 and performing the integration gives

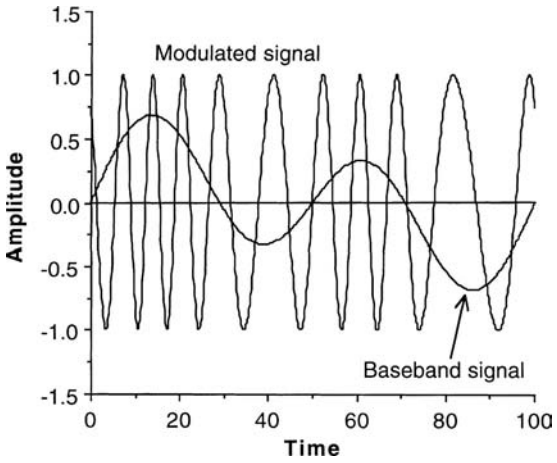

FIGURE 21.9 Time-domain representation of an FM signal and its baseband signal. The time scale is arbitrary.

$$f_s(t) = A_c \cos\left[\omega_c t + \beta \sin(\omega_m t)\right] \tag{21.15}$$

in which β (called the modulation index) has replaced $\Delta\omega A_m/\omega_m$. The carrier-quadrature form of Equation 21.15 is

$$f_s(t) = A_c\left\{\cos\left[\beta \sin(\omega_m t)\right]\cos(\omega_c t) - \sin\left[\beta \sin(\omega_m t)\right]\sin(\omega_c t)\right\} \tag{21.16}$$

We note from Equation 21.16 that, unlike AM, the FM signal contains both in-phase and quadrature components and that the amplitudes of both are nonlinear functions of the modulation index. The terms $\cos[\beta\sin(\omega_m t)]$ and $\sin[\beta\sin(\omega_m t)]$ are generally expanded in terms of Bessel functions (see Schwartz [3] for detailed analysis). The Bessel function expression of an FM signal is

$$f_s(t) = A_c \sum_{n=-\infty}^{\infty} J_n(\beta)\cos(\omega_c + n\omega_m)t \tag{21.17}$$

where J_n represents a Bessel function of the first kind of order n. Beyer [13] provides tables of $J_0(\beta)$ and $J_1(\beta)$ and gives formulae for computing higher-order Bessel functions. We also note that $J_{-n}(\beta) = (-1)^n J_n(\beta)$. The approximations $J_0(\beta) = 1$ and $J_1(\beta) = (\beta/2)$ are valid for low values of the modulation index ($\beta < 0.2$); the higher-order Bessel functions are negligible under these circumstances. A carrier with sinusoidal frequency modulation with a low modulation index will show sidebands spaced at $\pm\omega_m$ about the carrier; such narrowband FM would be indistinguishable from full-carrier AM on a spectrum analyzer display (which shows the amplitudes of spectral components but not their phase relationships). As modulation index increases, however, new sideband pairs appear at $\pm2\omega_m$, $\pm3\omega_m$, $\pm4\omega_m$, etc. as the higher-order Bessel functions become significant. The amplitude of the carrier component of $f_s(t)$ varies with $J_0(\beta)$; the carrier component disappears entirely for certain values of modulation index. These characteristics are unlike AM in which the carrier component of the modulated signal is constant and in which only one sideband pair is produced for each spectral component of the baseband signal. FM is an inherently nonlinear modulation process; the sum of multiple FM signals derived from a single carrier with individual baseband signals does not give the same result as frequency modulation of the carrier by the sum of the baseband signals. The spectrum of a phase-modulated signal is similar to that of an FM signal, but the modulation index of a phase-modulated signal does not vary with ω_m. Figure 21.9 shows a time-domain representation of an FM signal and the original baseband signal.

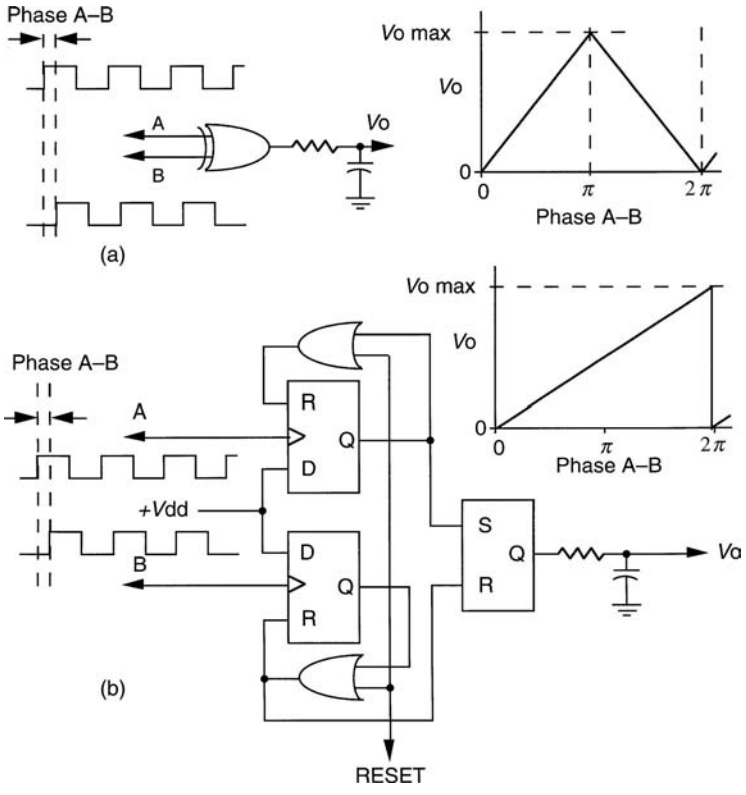

FIGURE 21.10 Examples of digital phase detectors. The exclusive-OR gate in (a) requires input signals with 50% duty cycle and produces an output voltage proportional to phase shift over the range of 0 to π radians (0° to 180°). Phase shifts between π and 2π radians produce an output voltage negatively proportional to phase. The edge-triggered RS flip-flop circuit in (b) functions with signals of arbitrary duty cycle and has a monotonic relationship between phase and output voltage over the full range of 0 to 2π radians. The circuit may be initialized by means of the RESET line. D-type flip-flops with RS capability (such as the CD4013) may be used in this circuit.

Generation of Phase- and Frequency-Modulated Signals

FM signals may arise directly in instrumentation systems such as turbine-type flowmeters or Doppler velocity sensors. Direct FM signals may be generated by applying the baseband signal to a voltage-controlled oscillator (VCO); Sherwin and Regan [14] demonstrate this technique in a system which generates direct FM using the LM566 VCO to transmit analog information over 60 Hz power lines. In radiofrequency applications, the oscillator frequency may be varied by application of the baseband signal to a voltage-variable reactance (such as a varactor diode). Indirect FM may be generated by phase modulation of the carrier by the integrated baseband signal as in Equation 21.14; DeFrance [15] gives an example of a phase modulator circuit.

Demodulation of Phase- and Frequency-Modulated Signals

PM signals may be demodulated by the synchronous demodulator circuits previously described; they are, however, sensitive to the signal amplitude as well as phase and require a limiter circuit to produce an output proportional to phase alone. Figure 21.10 shows simple digital phase demodulators. Figure 21.11 shows three of the more common methods of FM demodulation. Figure 21.11(a) shows a quadrature detector of the type commonly used in integrated-circuit FM receivers. A limiter circuit suppresses noise-induced amplitude variations in the modulated signal; the limiter output then provides a reference signal to a synchronous (phase-sensitive) demodulator. The limiter output voltage is also coupled (via a small

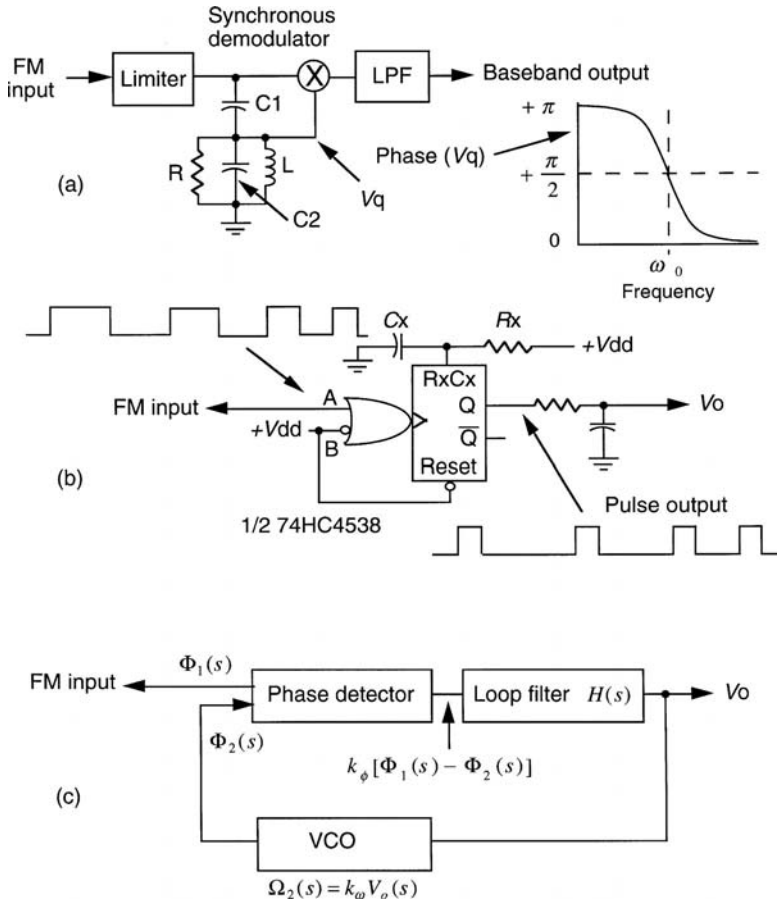

FIGURE 21.11 FM demodulators. A quadrature detector circuit is shown in (a). The phase shift of V_q (the voltage across the quadrature network consisting of *L*, *C*2, and *R*) relative to the output voltage of the limiter varies linearly with frequency for frequencies close to ω_0. The synchronous (phase-sensitive) demodulator produces an output proportional to the phase shift. A frequency-to-voltage converter is shown in (b). A monostable multivibrator (one-shot) produces a pulse of fixed width and amplitude with each cycle of the modulated signal. The average voltage of these pulses is proportional to the modulated signal frequency. The 74HC4538 contains two independent edgetriggered monostable multivibrators which may be triggered by a rising edge (as shown) or a falling edge (by applying the clock pulse to the B input and connecting the A input to V_{dd}). A phase-locked loop is shown in (c). The operation of the phase-locked loop is described in the text.

capacitor *C*1) to a quadrature network consisting of *L*, *R*, and *C*2. The phase of the voltage across the quadrature network relative to the limiter output is given by

$$\phi\left[V_q(\omega)\right] = \tan^{-1}\frac{-\omega L/R}{\left[1-\left(\omega/\omega_0\right)^2\right]} \tag{21.18a}$$

where

$$\omega_0 = \frac{1}{\sqrt{L\left(C_1 + C_2\right)}} \tag{21.18b}$$

The variation in phase is nearly linear for frequencies close to ω_0. The phase-sensitive demodulator recovers the baseband signal from the phase shift between the quadrature-network voltage and the reference signal. The quadrature network also causes the amplitude of V_q to vary with frequency, but the variation in phase with respect to frequency predominates over amplitude variation in the vicinity of ω_0. There is also generally enough voltage across the quadrature network to force the phase-sensitive demodulator into a nonlinear regime in which its output voltage is relatively insensitive to the amplitude of the voltage across the quadrature network. Figure 21.11(b) shows a frequency-to-voltage converter which consists of a monostable (one-shot) triggered on each zero crossing of the modulated signal. The pulse output of the one-shot is integrated by the low-pass filter to recreate the original baseband signal. Figure 21.11(c) shows a phase-locked loop. The phase comparator circuit produces an output voltage proportional to the phase difference between the input signal and the output of a VCO; that voltage is filtered and used to drive the VCO. Assume that $\phi_1(t)$ and $\omega_1(t)$ represent the phase and frequency of the input signal as functions of time with corresponding Laplace transforms $\Phi_1(s)$ and $\Omega_1(s)$. The VCO output phase and frequency are represented by $\phi_2(t)$ and $\omega_2(t)$ with corresponding Laplace transforms $\Phi_2(s)$ and $\Omega_2(s)$. The phase detector produces an output voltage given by

$$v_\phi(t) = k_\phi\left[\phi_1(t) - \phi_2(t)\right] \tag{21.19}$$

The corresponding Laplace transform expression is

$$V_\phi(s) = k_\phi\left[\Phi_1(s) - \Phi_2(s)\right] \tag{21.20}$$

This voltage is filtered by the loop filter and is applied to the VCO which produces a frequency proportional to the control voltage. The Laplace transform of the VCO frequency is

$$\Omega_2(s) = k_\omega k_\phi H(s)\left[\Phi_1(s) - \Phi_2(s)\right] \tag{21.21}$$

Since $\Phi_1(s) = \Omega_1(s)/s$ and $\Phi_2(s) = \Omega_2(s)/s$, we may write

$$\Omega_2(s) = \left[\frac{k_\omega k_\phi H(s)}{s + k_\omega k_\phi H(s)}\right]\Omega_1(s) \tag{21.22}$$

Assume that the input frequency is a step function of height ω_1; this gives $\Omega_1(s) = \omega_1/s$. Inserting this into Equation 21.22 gives

$$\Omega_2(s) = \left[\frac{k_\omega k_\phi H(s)}{s + k_\omega k_\phi H(s)}\right]\frac{\omega_1}{s} \tag{21.23}$$

Application of the final value theorem of the Laplace transform to Equation 21.24 gives ω_1 as the asymptotic limit of $\omega_2(t)$; the output frequency of the VCO matches the input frequency. The VCO input voltage is ω_1/k_ω and is thus proportional to the input frequency. If the input frequency is varied by some baseband signal, the VCO input voltage follows that baseband signal. The phase-locked loop thus may serve as an FM detector; Taub and Schilling [2] give an extensive analysis. If we assume the simplest loop filter transfer function $H(s) = 1$, the bracketed term of Equation 21.21 takes the form of a single-pole low-pass filter with corner frequency $\omega_{-3dB} = k_\omega k_\phi$. The VCO output frequency tracks slowly varying input frequencies quite well, but the response to rapidly varying input frequencies is limited by the low-pass behavior of the loop. Baseband spectral components which lie below the loop corner frequency are recovered without distortion, but baseband spectral components beyond the loop corner frequency are

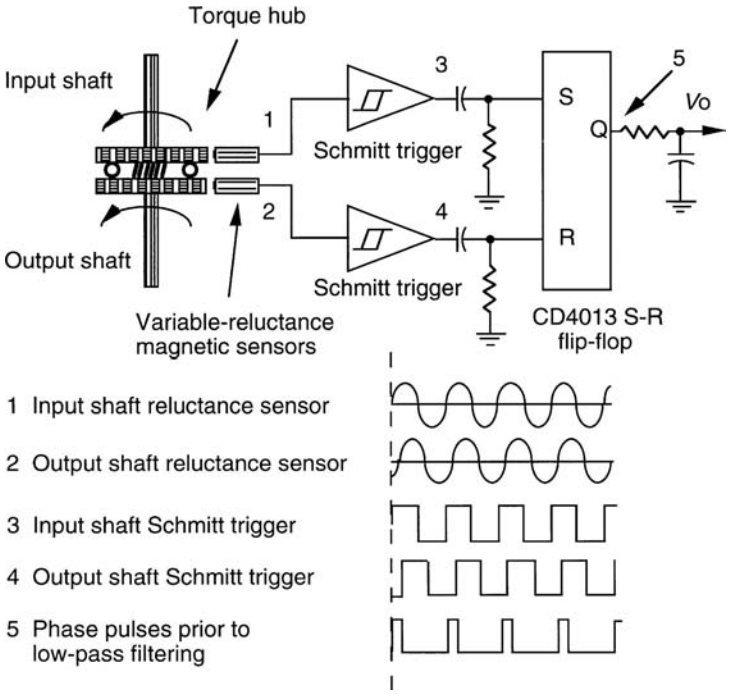

FIGURE 21.12 Use of phase-sensitive demodulation to measure torque in a rotating shaft as described by Sokol et al. [16]. Typical waveforms and the points in the circuit where they are found are indicated. The *RC* coupling to the S and R terminals of the CD4013 flip-flop provides for edge triggering.

attenuated. A single-pole *RC* low-pass filter is often used for the loop filter; the transfer function of the complete phase-locked loop with such a filter is:

$$\frac{\Omega_2(s)}{\Omega_1(s)} = \left[\frac{k_\omega k_\phi p_1}{s^2 + sp_1 + k_\omega k_\phi p_1}\right] \tag{21.24}$$

where $p_1 = 1/RC$. Note that the loop transfer function is that of a second-order low-pass filter and thus may exhibit dynamics such as resonance and underdamped transient response depending on the values of the parameters k_ω, k_ϕ, and p_1.

Examples

Sokol et al. [16] describe the use of phase-sensing techniques to a shaft torque-sensing application in Figure 21.12. Two identical gears are coupled by springs in a device known as a torque hub. The teeth of the gears induce signals in variable-reluctance magnetic sensors as the shaft rotates, and the Schmitt trigger circuits transform the reluctance sensor outputs (approximately sinusoidal signals with amplitudes proportional to shaft rotational velocity) into square waves of constant amplitude. The springs compress with increasing torque, shifting the phase of the magnetic pickup signals (and hence the square waves) relative to each other. The relative phase of the square waves is translated to a dc voltage by a flip-flop phase detector and *RC* low-pass filter. The suppression of amplitude variation by the Schmitt trigger circuits causes no loss of information; the torque measurement is conveyed by phase alone.

Cohen et al. [17] in Figure 21.13 describe the use of a direct FM technique to perform noninvasive monitoring of human ventilation. Elastic belts with integral serpentine inductors encircle the chest and abdomen; these inductors are parts of resonant tank circuits of free-running radiofrequency oscillators. Ventilation causes the inductor cross-sectional areas to vary, changing their inductances and thus varying

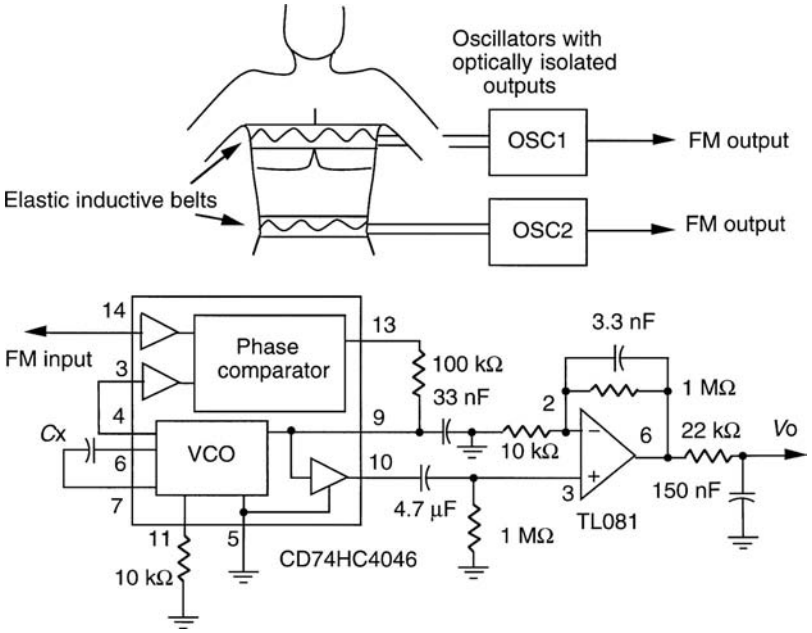

FIGURE 21.13 Use of FM techniques in measurement of human ventilation (adapted from Cohen et al. [17]). An independent oscillator was used for each inductive belt, and the oscillator outputs were optically coupled to the demodulator circuits for the purpose of electrical isolation of the subject from equipment operated from the 60 Hz ac line. One of two demodulators is shown; the value of C_x was either 470 pF for use at a nominal frequency of 850 kHz or 220 pF for use at a nominal frequency of 1.5 MHz. Numbers adjacent to the CD74HC4046 and TL081 devices are pin numbers.

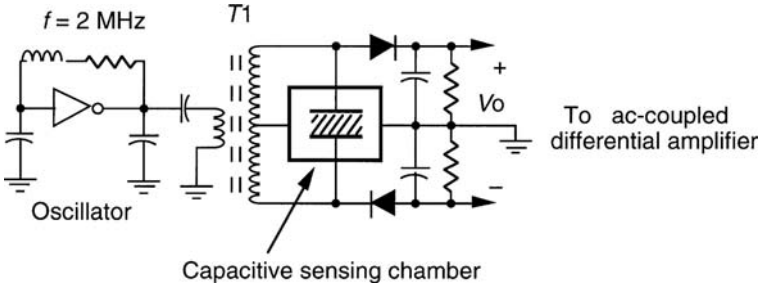

FIGURE 21.14 FM demodulator technique applied to measurement of the flow of small seeds in an agricultural machine application. The relative permittivity of the seeds causes the resonant frequency of the discriminator circuit to shift and to produce a change in the output voltage. The claimed sensitivity of this circuit is on the order of tens of femtofarads. The cross-hatched region of the sensing chamber represents the active area through which the seeds flow.

the frequencies of the oscillators. Figure 21.13 also shows one of two phase-locked loop demodulator circuits which are identical except for the value of one capacitor in the VCO circuit. The phase-locked loop utilizes a single-pole *RC* low-pass loop filter.

Bachman [18,19] in Figure 21.14 describes a novel application of FM techniques to provide a sensing function which would otherwise be difficult to achieve (measurement of deviations in mass flow of fine seeds in an agricultural implement). A capacitive sensing cell was constructed and made part of a discriminator circuit driven at a constant frequency; the flow of seeds through the sensing capacitor shifts the resonant frequency of the discriminator and produces a change in the discriminator output voltage. An ac-coupled differential amplifier provides an output proportional to changes in the mass flow.

TABLE 21.1 Integrated Circuits Used with Modulation Techniques

Designation	Function	Manufacturer(s)	Approximate Price, $
AD630JN	Balanced modulator/demodulator	Analog Devices	10.19
74HC4053	High-speed analog switch	Fairchild, TI	0.67
ADG201HSJN	High-speed analog switch	Analog Devices	3.10
AD532JH	Four-quadrant multiplier	Analog Devices	15.91
AD633JN	Four-quadrant multiplier	Analog Devices	3.73
74HC4046	Phase-locked loop	Fairchild, TI	2.00
AD650JN	Voltage-to-frequency, frequency-to-voltage converter	Analog Devices	9.15
AD652JP	Voltage–to-frequency converter	Analog Devices	10.46
AD654JN	Voltage-to-frequency converter	Analog Devices	4.15
74HC4538	Dual retriggerable monostable (one-shot)	Fairchild, TI	0.72

TABLE 21.2 Companies That Make Integrated Circuits for Modulating

Analog Devices, Inc.
One Technology Way
Box 9106
Norwood, MA 02062
Phone: (617) 329-4700
www.analog.com

Fairchild Semiconductor Corp.
82 Running Hill Road
South Portland, ME 04106
Phone: (207) 775-8100
www.fairchildsemi.com

Texas Instruments, Inc.
12500 TI Blvd.
Dallas, TX 75243-4136
www.ti.com

21.5 Instrumentation and Components

Integrated Circuits

Table 21.1 lists certain integrated circuits which may be used in application of the modulation techniques covered in this chapter. This is not an exhaustive list of all useful types nor of all manufacturers. Most integrated circuits are available in a number of packages and performance grades; the prices given are indicative of the pricing of the least expensive versions purchased in small quantities. Table 21.2 provides contact information for these vendors.

Instrumentation

Oscilloscopes and spectrum analyzers are frequently employed in analysis of modulated signals or systems utilizing modulation techniques; both types of instruments are available from a number of manufacturers (e.g., Agilent Technologies, Tecktronix). Certain types of specialized instrumentation are also available, such as scalar and vector modulation analyzers, signal sources with digital or analog modulation capability, and instruments for analysis of color-television signals (vectorscopes). Representative manufacturers include Agilent Technologies, Tektronix, and Rohde & Schwarz. Additional information is available from their respective on-line sources.

Defining Terms

Modulation: The process of encoding the source information onto a bandpass signal with a carrier frequency f_c.

Amplitude modulation (AM): Continuous wave modulation, where the amplitude of the carrier varies linearly with the amplitude of the modulating signal.

Angle modulation: Continuous wave modulation, where the angle of the carrier varies linearly with the amplitude of the modulating signal.

Frequency modulation (FM): Continuous wave modulation, where the frequency of the carrier varies linearly with the amplitude of the modulating signal.

References

1. A.B. Carlson, *Communication Systems,* 3rd ed., New York: McGraw-Hill, 1986.
2. H. Taub and D.L. Schilling, *Principles of Communication Systems,* New York: McGraw-Hill, 1971.
3. M. Schwartz, *Information Transmission, Modulation, and Noise,* 4th ed., New York: McGraw-Hill, 1990.
4. W. Tomasi, *Advanced Electronic Communications Systems,* 2nd ed., Englewood Cliffs, NJ: Prentice-Hall, 1992.
5. D.J. Nowicki, Voltage measurement and signal demodulation, in J. G. Webster, Ed., *Electrical Impedance Tomography,* Bristol, UK: Adam Hilger, 1990.
6. M.L. Meade, *Lock-in Amplifiers: Principles and Applications*, London: Peregrinus, 1984.
7. J.G. Webster, Ed., *Electrical Impedance Tomography,* Bristol, UK: Adam Hilger, 1990.
8. D.L. Hershberger, Build a synchronous detector for AM radio, *Pop. Electron.*, 20 (4), 61, 66–71, 1982.
9. G.A. Breed, Receiver basics—part 2. Fundamental receiver architectures, *RF Design*, 17 (3), 84, 86, 88–89, 1994.
10. Anonymous, AD630 balanced modulator/demodulator, in *Analog Devices* 1992 *Special Linear Reference Manual,* pp. 2.35–2.41, 1992.
11. J.G. Webster, Ed., *Medical Instrumentation: Application and Design.,* 3rd ed., New York: John Wiley & Sons, 1998.
12. D.M. Beams. Project TUNA — the development of a LabVIEW virtual instrument as a class project in a junior-level electronics course, *Comput. Educ. J.* 11, 1, 28–33, 2001. Additional information available at http://www.eng.uttyl.edu/usr/dbeams/home/Tuna/Project_TUNA.htm.
13. W.H. Beyer, *CRC Standard Mathematical Tables,* 28th ed., Boca Raton, FL: CRC Press, 1987.
14. J. Sherwin and T. Regan, FM remote speaker system, National Semiconductor Application Note AN-146, in *National Semiconductor Corp.* 1991 *Linear Applications Databook,* 1991.
15. J.J. DeFrance, *Communication Electronics Circuits,* 2nd ed., San Francisco, CA: Rinehart Press, 1972.
16. D.G. Sokol, R.B. Whitaker, J.J. Lord, and D.M. Beams, *Combine data center,* U.S. Patent No. 4,376,298, 1983.
17. K.P. Cohen, D. Panescu, J.H. Booske, J.G. Webster, and W.J. Tompkins, Design of an inductive plethysmograph for ventilation measurement, *Physiol. Meas.,* 15, 217–229, 1994.
18. W.J. Bachman, *Capacitive-type seed sensor for a planter monitor,* U.S. Patent No. 4,782,282, 1988.
19. W.J. Bachman, Private communication, 1995.